AIAA Aviation
16-20 June 2014, Atlanta, GA
32nd AIAA Applied Aerodynamics Conference

Co-Flow Jet Airfoil Trade Study Part II : Moment and Drag

Alexis Lefebvre *, G.-C. Zha †
Dept. of Mechanical and Aerospace Engineering
University of Miami
Coral Gables, Florida 33124
E-mail: gzha@miami.edu

Abstract

This paper is Part II of a parametric study on CFJ airfoils. In the first part of the paper, the CFJ airfoil suction surface shape is modified to reduce or overcome the nose-down moment. In the second part of the paper, the injection and suction sizes and C_μ are varied to increase the CFJ airfoil thrust generation. For both parts, the resulting effects on the lift, drag, moment and energy consumption is analyzed. The two dimensional flow is simulated using steady and unsteady Reynolds Average Navier-Stokes (RANS). A 5th order WENO scheme for the inviscid flux, a 4th order central differencing model for the viscous terms and the one equation Spalart-Allmaras model for the turbulence are used to resolve the flow. The Mach number is 0.15 and Reynolds number is 6.4×10^6. The nose-down moment of the CFJ airfoils was successfully reduced with the use of reflex camber while negative drag was achieved with a thinner airfoil, and a reduced injection size. Increasing C_μ further reduces the drag, but at the cost of a much higher energy consumption and reduced corrected aerodynamic efficiency. The minimum drag achieved is $C_D = -0.033$ and the highest moment achieved is $C_M = 0.031$.

* Graduate Student
† Professor, AIAA Associate Fellow

Nomenclature

CFJ	Co-flow jet
AoA	Angle of attack
LE	Leading Edge
TE	Trailing Edge
S	Planform area
c	Profile chord
U	Flow velocity
q	Dynamic pressure $0.5\,\rho\,U^2$
p	Static pressure
ρ	Air density
$\dot{m}$	Mass flow
M	Mach number
ω	Pitching Moment
P	Pumping power
∞	Free stream conditions
$_j$	Jet conditions
C_L	Lift coefficient $L/(q_\infty\,S)$
C_D	Drag coefficient $D/(q_\infty\,S)$
C_M	Moment coefficient $\omega/(q_\infty\,S\,c)$
C_p	Pressure coefficient $(p-p_\infty)/q_\infty$
C_μ	Jet momentum coef. $\dot{m}_j\,U_j/(q_\infty\,S)$
$(L/D)_c$	CFJ airfoil corrected efficiency $L/(D\,P/V_\infty)$
Pc	Power coefficient $L/(q_\infty\,S\,V_\infty)$

1 Introduction

A high performance airfoil should have a combination of high maximum lift, high cruise L/D and relatively low nose-down moment for stability. To enhance the maximum lift the use of flaps and slats are often necessary. The NACA 23021 airfoil with two different flap configurations have been experimentally studied by T. A. Harris in [1]. The maximum C_L achieved by the slotted flapped airfoil with a large flap deflection is 2.49. However the very high C_D of 0.17 and C_M of -0.37 render this performance point unusable in practice. A more reasonable flap deflection angle achieved a maximum C_L of 2.0 with an associated C_D of 0.045 and C_M of -0.39 for the best configuration. The flapped configuration suffers from an important drag and nose-down moment that reduces the airfoil aerodynamic efficiency and requires important tail force to balance, further reducing the airplane efficiency. In addition, those devices introduce a significant weight penalty and complexity in the wing structure.

Recently, a zero-net mass-flux(ZNMF) co-flow jet (CFJ) flow control airfoil developed by Zha et al. [2, 3, 4, 5, 6, 7, 8, 9, 10] based on fluidic actuators is demonstrated to achieve radical lift augmentation, stall margin increase, drag reduction and moderate nose-down moment for stationary and pitching airfoils. In the CFJ airfoil concept an injection slot near the leading edge (LE) and a suction slot near the trailing edge (TE) on the airfoil suction surface are created as sketched in Fig. 1. A small mass flow is withdrawn into the airfoil near the TE, pressurized and energized by a pumping system inside the airfoil, and then injected near the LE tangentially to the main flow. The whole process does not add any mass flow to the system and hence is a ZNMF flow control. The energy expenditure is low [3, 8, 9] and the implementation is straightforward.

The Part I of the parametric study [11] focused on the energy consumption and corrected aerodynamic efficiency

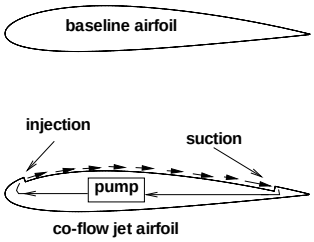

Figure 1: CFJ airfoil concept

via a trade study performed for a NACA 23121 CFJ airfoil on the injection and suction location and size, AoA, C_μ, airfoil thickness and Reynolds number. The distinguishing feature of CFJ airfoil from conventional non-controlled airfoil is that CFJ airfoil gain the efficiency benefit at high C_L range, where the conventional non-controlled airfoil can not reach due to stall. The injection location and the AoA are found to be the influential parameters. The pitch-down moment and energy consumption are decreased by using an upstream suction location while the more downstream location benefit the lift and drag. The energy consumption is decreased with the increasing AoA and reaches a minimum of $Pc = 0.033$ at $AoA = 25°$ for a suction location of 40% chord and $C_\mu = 0.16$. For the same C_μ, the maximum lift coefficient is 2.91 at $AoA = 32.5°$ and the minimum drag coefficient is 0.003 at $AoA = 0.0°$.

This Part II parametric study, focuses on the nose-down moment and drag reduction of CFJ airfoils. The NACA 23121, NACA 34121 and NACA 6321 CFJ airfoils, are modified to reduce the nose-down moment. Then the NACA23112 identified in the PART I trade study as the best candidate to achieve negative drag and high efficiency is investigated for various C_μ and injection sizes.

2 CFJ Parameters

This section will introduce the definitions of several parameters that are important for CFJ airfoil performance.

2.1 Lift and Drag Calculation

The momentum and pressure at the injection and suction slots produce a reactionary force, which is automatically measured by the force balance in wind tunnel testing. However, for CFD simulation, the full reactionary force needs to be included. Using control volume analysis, the reactionary force can be calculated using the flow parameters at the injection and suction slot opening surfaces. Zha et al. [3] give the following formulations to calculate the lift and drag due to the jet reactionary force for a CFD simulation. By considering the effects of injection and suction jets on the CFJ airfoil, the expressions for these reactionary forces are given as :

$$F_{x_{cfj}} = (\dot{m}_j V_{j1} + p_{j1} A_{j1}) * cos(\theta_1 - \alpha) - (\dot{m}_j V_{j2} + p_{j2} A_{j2}) * cos(\theta_2 + \alpha) \tag{1}$$

$$F_{y_{cfj}} = (\dot{m}_{j1} V_{j1} + p_{j1} A_{j1}) * sin(\theta_1 - \alpha) + (\dot{m}_{j2} V_{j2} + p_{j2} A_{j2}) * sin(\theta_2 + \alpha) \tag{2}$$

where the subscripts 1 and 2 stand for the injection and suction respectively, and θ_1 and θ_2 are the angles between the injection and suction slot's surface and a line normal to the airfoil chord. α is the angle of attack.

The total lift and drag on the airfoil can then be expressed as:

$$D = R'_x - F_{x_{cfj}} \tag{3}$$

$$L = R'_y - F_{y_{cfj}} \tag{4}$$

where R'_x and R'_y are the surface integral of pressure and shear stress in x (drag) and y (lift) direction excluding the internal ducts of injection and suction. For the CFD simulation, the total lift and drag are calculated using Eqs.(3) and (4).

2.2 Jet Momentum Coefficient

The jet momentum coefficient C_μ is a parameter used to quantify the jet intensity. It is defined as :

$$C_\mu = \frac{\dot{m}V_j}{\frac{1}{2}\rho_\infty {V_\infty}^2 S} \tag{5}$$

where $\dot{m}$ is the injection mass flow, V_j the injection velocity, ρ_∞ and V_∞ denote the free stream density and velocity, and S is the planform area.

2.3 Power Coefficient

The CFJ can be implemented by mounting a pumping system inside the wing that withdraws air from the suction slot and blows it into the injection slot. The power consumption can be determined by the jet mass flow and total enthalpy change as the following :

$$P = \dot{m}(H_{t1} - H_{t2}) \tag{6}$$

where H_{t1} and H_{t2} are the total enthalpy in the injection cavity and suction cavity respectively, P is the Power required by the pump and $\dot{m}$ the jet mass flow rate. Introducing the pump efficiency η and total pressure ratio of the pump $\Gamma = \frac{P_{t1}}{P_{t2}}$, the power consumption can be expressed as :

$$P = \frac{\dot{m}C_p T_{t2}}{\eta}(\Gamma^{\frac{\gamma-1}{\gamma}} - 1) \tag{7}$$

The power consumption can be expressed as a power coefficient below:

$$P_c = \frac{P}{\frac{1}{2}\rho_\infty V_\infty^3 S} \tag{8}$$

2.4 Corrected Aerodynamic Efficiency

The conventional airfoil aerodynamic efficiency is defined as :

$$\frac{L}{D} \tag{9}$$

For the CFJ airfoil, this ratio still represents the aerodynamic efficiency in the sense of pure aerodynamic forces. However since CFJ active flow control consumes energy, the CFJ corrected aerodynamic efficiency is modified to

take into account the energy consumption of the pump. The formulation of the corrected aerodynamic efficiency for CFJ airfoils is :

$$(\frac{L}{D})_c = \frac{L}{D + \frac{P}{V_\infty}} \tag{10}$$

where V_∞ is the free stream velocity, P is the pumping power, and L and D are the lift and drag generated by the CFJ airfoil. This formulation converts the power consumed by the CFJ into the drag of the airfoil. If the pumping power is set to 0, this formulation returns to the formulation of a conventional airfoil.

3 CFD Simulation Setup

3.1 CFD Code

The FASIP (Flow-Acoustics-Structure Interaction Package) CFD code is used to conduct the numerical simulation. The 2D Reynolds averaged Navier-Stokes (RANS) equations with one-equation Spalart-Allmaras [12] turbulence model is used. A 5th order WENO scheme for the inviscid flux [13, 14, 15, 16, 17, 18] and a 4th order central differencing for the viscous terms [13, 17] are employed to discretize the Navier-Stokes equations. The low diffusion E-CUSP scheme used as the approximate Riemann solver suggested by Zha et al [14] is utilized with the WENO scheme to evaluate the inviscid fluxes. Implicit time marching method using Gauss-Seidel line relaxation is used to achieve a fast convergence rate [19]. Parallel computing is implemented to save wall clock simulation time [20]. The RANS solver is validated for CFJ static airfoil simulation [6, 9, 21, 22].

3.2 Boundary Conditions

The 3rd order accuracy no slip condition is enforced on the solid surface with the wall treatment suggested in [23] to achieve the flux conservation on the wall. Total pressure, total temperature and flow angles are specified as the inlet boundary conditions for the upstream portion of the farfield boundary and inside the injection cavity. Constant static pressure is used for the downstream portion of the farfield boundary and inside the suction cavity.

To achieve zero net mass flux with the CFJ flow control, the mass flow exiting the injection slot must be equal to the mass flow entering the suction slot. Additionally, the jet strength must be controlled in order to reach the prescribed C_μ. The prescribed C_μ is achieved by adjusting the injection cavity total pressure. Total temperature is assumed constant during this process. The injection and suction mass flow are matched by adjusting the suction cavity static pressure. The process is iterated throughout the simulation until the specified momentum coefficient is reached and the injection and suction mass flow match within the tolerance of 1%.

3.3 Mesh

The NACA 23121 CFJ airfoil grid (Fig. 2) is constructed using the O-mesh topology in order to achieve high quality around the airfoil. The mesh uses a total of 330 points around airfoil partitioned into 210 points on the suction surface and 120 points on the pressure surface, 180 points are placed in the direction normal to the airfoil with an additional 60 points across the jet. The total mesh size is 75,600 cells and the mesh is splitted into 14 blocks for the parallel computation. The farfield boundary is located 30 chords away from the airfoil. The first grid point is placed at $y^+ \approx 1$ to resolve the turbulent boundary layer.

A refined grid is constructed using 50% more points in every direction and $y^+ \approx 0.7$. The refined mesh results agree well with the original meshes.

4 Results

4.1 Low Moment CFJ Airfoils

The suction surface of the NACA 23121, NACA 34121 and NACA 6321 CFJ airfoils is modified to reduce or overcome the nose-down moment and the resulting aerodynamic performance and efficiency is quantified. The airfoils injection and suction slots are located at 6% and 40% chord respectively. Injection and suction slot sizes are 0.75% and 1.35% chord. Because of the large number of geometries created for this section, this study focuses on $AoA = 10°$ and $C_\mu = 0.16$.

The NACA 23121, NACA 34121 and NACA 6321 CFJ airfoil variations are shown in Fig. 3. All the injection and suction cavities are the same as in Fig. 2 though are not plotted in Fig. 3 for clarity. For all the cases, variation 0 is constructed from the NACA baseline airfoil by lowering the suction surface between the injection and suction slot. The variation 1 airfoil is generated from variation 0 by decreasing the injection angle by 0.5° for the NACA 23121 and NACA 34121 and by 1.0° for the NACA 6321. Doing so also rotates the suction surface downstream of the injection. Reflex camber is then used in the last 20% of the airfoil to link the rotated suction surface to the TE. Variations 2,3 and 4 are constructed similarly by increasing the rotation angle of the suction surface and reflex camber. The injection angle is lowered by 2.0° for the NACA 23121 and NACA 34121, and 4.0° for the NACA 6321. For all the variations the airfoil nose and pressure surface remain unchanged.

The forces, moment and power consumption for the CFJ airfoil variations are displayed from Fig. 4 to Fig. 6. The NACA 23121 CFJ airfoil lift coefficient is decreased from 1.34 for variation 0 to 1.19 for variation 4 due to the use of increasing reflex camber. Interestingly, the drag is reduced as well because the pressure repartition of reflex airfoils features a higher back pressure that reduces the pressure drag. In addition, the slightly more horizontal injection generates more thrust. The power consumption decreases with the variation number because of the slightly lower injection pressure, however, the decrease of the power consumption and the drag are not enough to compensate for the decrease of lift, and the $(L/D)_c$ is reduced from 18.1 to 17.2. L/D is excellent for all variations and ranges between 120.0 and 121.1, a 65% increase over the baseline airfoil value. The NACA 23121 CFJ airfoil variation 1 shows that for a modest concession on the corrected aerodynamic efficiency the moment can be significantly improved. Similar conclusion are found for the NACA 6321 and NACA 34121 CFJ airfoils.

Unlike the NACA 6321 CFJ airfoil, the NACA 23121 and 34121 CFJ airfoil moments vary from negative to positive among the variations. The NACA 23121 variation 1 and NACA 34121 variation 2 airfoils achieved a neutral moment. When comparing those two low moment airfoils, there is a significant advantage in term of corrected aerodynamic efficiency for the NACA 23121 variation ($(\frac{L}{D})_c$ 17.9 vs 16.5) due to the combined effects of a higher lift, a smaller drag and reduced power consumption.

4.2 CFJ Airfoil with Thrust Generation

The low drag NACA 21112 CFJ thin airfoil studied in [11] is simulated with varying AoA, C_μ and injection sizes and the resulting aerodynamic performance and efficiency is quantified. The airfoils injection and suction slots are located at 4% and 40% chord respectively. The injection and suction slot sizes are 0.75% and 1.35% chord for the original injection size and 0.50% and 1.00% for the smaller injection size.

The CFJ airfoils studied for thrust generation are shown in Fig. 5. The NACA 23112 CFJ airfoil is chosen with an injection location moved upstream to 4% chord location because this thin airfoil features a low drag and a high efficiency in the thickness trade study form [11].

The AoA and C_μ of the NACA 23112 CFJ airfoil are varied and the corresponding forces, moment and power consumption are displayed in Fig. 8. The results are compared with the simulated baseline airfoil with no CFJ. At high AoA, unsteady simulations are conducted to capture the boundary-layer separation and turbulent mixing.

The lift is greatly enhanced by the use of CFJ even though the improvement is not as significant as with the thick NACA 23121 CFJ airfoil [11] because the lower thickness reduces the circulation. The maximum lift coefficient reaches $C_Lmax = 2.40$ for $C_\mu = 0.16$, a significant improvement compared with the baseline airfoil that reaches a maximum C_Lmax of 1.50. The CFJ airfoil stall pattern is much sharper than with the NACA 23121 CFJ airfoil ([11]). The CFJ airfoil drag coefficient remains negative until $AoA \approx 11^\circ$ at $C_\mu = 0.16$ with a minimum value of $C_Dmin = -0.019$. The moment coefficient remains fairly flat until $AoA \approx 15^\circ$ and increases for higher AoA at $C_\mu = 0.12$ and $C_\mu = 0.16$ because of a flow separation developing at the airfoil TE at high AoA. The stall pattern is different at $C_\mu = 0.08$. The weaker jet is unable to overcome the large adverse pressure gradient at the LE and the airfoil stalls with a separation starting at the LE. The power consumption is decreased with the increasing AoA before the separation occurs. This phenomenon is confirmed by the wind tunnel testing in [24] and the simulations in [9]. The mechanism is that when the AoA increases, the LE suction is stronger and the pressure of the main flow surrounding the injection slot is lower, hence reducing the pumping power to generate the jet. When the AoA is too high however, the jet total pressure loss is increased due to the large adverse pressure gradient and flow separation. At $C_\mu = 0.16$, the corrected aerodynamic efficiency and power consumption of the CFJ airfoil reach $(\frac{L}{D})_c = 35.3$ and $Pc = 0.043$. Those values are considerably improved for lower C_μ and with $(\frac{L}{D})_c = 64.4$ and $Pc = 0.011$ at $C_\mu = 0.08$. The pure aerodynamic efficiency is tremendously improved for the CFJ airfoil and reaches close to $L/D = 300$ at $C_\mu = 0.08$. At higher C_μ, the maximum L/D reached is infinity when the drag is null.

The NACA 23112 CFJ airfoil injection and suction slot size are reduced by 1/3 and the corresponding forces, moment and power consumption are displayed in Fig. 9. The lift and drag are significantly improved for the smaller injection size when compared to the original injection size and reach $C_Lmax = 2.81$ and $C_Dmin = -0.033$ at $C_\mu = 0.16$. The drag is negative until $AoA \approx 16^\circ$ at $C_\mu = 0.16$. The moment is similar to the original injection size for $C_\mu = 0.12$ and $C_\mu = 0.16$. For $C_\mu = 0.08$ the LE stall pattern observed for the original injection size is not observed here because the smaller injection slot generates a faster jet that enhances the mixing with the main flow, thereby increasing the performance and better prevents the LE flow separation. On the other hand, the smaller and faster jet loses more total pressure by friction, and mixing with the main flow and the pumping power is increased. The drag reduction and lift enhancement are not enough to balance the power increase and the corrected aerodynamic efficiency is decreased to $(\frac{L}{D})_c = 28.9$ and $Pc = 0.068$ at $C_\mu = 0.16$. Those values are considerably improved for lower C_μ with $(\frac{L}{D})_c = 51.9$ and $Pc = 0.018$ at $C_\mu = 0.08$. The pure aerodynamic efficiency L/D is tremendously improved for the CFJ airfoil and reaches infinity when the drag is null.

The corrected aerodynamic efficiency versus C_D plot shown in Fig. 10 indicates that the more thrust the airfoil generates, the lower the efficiency. The smaller injection size achieves negative drag more efficiently than the original injection size.

5 Conclusion

This Part II parametric study focuses on the nose-down moment and drag reduction of CFJ airfoils. In the first part of the paper, the CFJ airfoil suction surface shape is modified to reduce or overcome the nose-down moment. In the second part of the paper, the injection and suction sizes and C_μ are varied to increase the CFJ airfoil thrust generation. The nose-down moment of the CFJ airfoils is reduced with the use of reflex camber while negative drag is achieved with good efficiency using a thin airfoil with a small injection size. Increasing C_μ further reduces the drag but at the cost of a much higher energy consumption and reduced corrected aerodynamic efficiency. The minimum drag achieved is $C_D = -0.033$ and the highest moment achieved is $C_M = 0.031$. The thrust generation and low moment are desirable characteristics for a distributed propulsion system that could potentially remove the need for conventional propulsion.

References

[1] T. A. Harris and R. S. Swanson, "Wind-tunnel tests of an NACA 23021 airfoil equipped with a slotted extensible and plain extensible flap ." Technical Note No. 782, NACA, November 1940.

[2] G.-C. Zha and D. C. Paxton, "A Novel Flow Control Method for Airfoil Performance Enhancement Using Co-Flow Jet." *Applications of Circulation Control Technologies*, Chapter 10, p. 293-314, Vol. 214, Progress in Astronautics and Aeronautics, AIAA Book Series, Editors: Joslin, R. D. and Jones, G.S., 2006.

[3] G.-C. Zha, W. Gao, and C. Paxton, "Jet Effects on Co-Flow Jet Airfoil Performance," *AIAA Journal, No. 6,*, vol. 45, pp. 1222–1231, 2007.

[4] G.-C. Zha, C. Paxton, A. Conley, A. Wells, and B. Carroll, "Effect of Injection Slot Size on High Performance Co-Flow Jet Airfoil," *AIAA Journal of Aircraft*, vol. 43, 2006.

[5] G.-C. Zha, B. Carroll, C. Paxton, A. Conley, and A. Wells, "High Performance Airfoil with Co-Flow Jet Flow Control," *AIAA Journal*, vol. 45, 2007.

[6] Wang, B.-Y. and Haddoukessouni, B. and Levy, J. and Zha, G.-C., "Numerical Investigations of Injection Slot Size Effect on the Performance of Co-Flow Jet Airfoil," *Journal of Aircraft*, vol. 45, No. 6, pp. 2084–2091, 2008,.

[7] B. P. E. Dano, D. Kirk, and G.-C. Zha, "Experimental Investigation of Jet Mixing Mechanism of Co- Flow Jet Airfoil." AIAA-2010-4421, 5th AIAA Flow Control Conference, Chicago, IL, 28 Jun - 1 Jul 2010.

[8] B. P. E. Dano, G.-C. Zha, and M. Castillo, "Experimental Study of Co-Flow Jet Airfoil Performance Enhancement Using Micro Discreet Jets." AIAA Paper 2011-0941, 49th AIAA Aerospace Sciences Meeting, Orlando, FL, 4-7 January 2011.

[9] A. Lefebvre, B. Dano, M. D. Fronzo, W. B. Bartow, and G-C. Zha, "Performance of a Co-Flow Jet Airfoil with Variation of Mach Number," *AIAA paper 2013-490*, Jan 2013.

[10] A. Lefebvre, G-C. Zha, "Numerical Simulation of Pitching Airfoil Performance Enhancement Using Co-Flow Jet Flow Control," *AIAA paper 2013-2517*, June 2013.

[11] A. Lefebvre, G-C. Zha, "Cow-Flow Jet Airfoil Trade Study Part I : Energy Consumption and Aerodynamic Performance," *Proceedings of the AIAA Flow Control Conference*, June 2014.

[12] P. Spalart and S. Allmaras, "A One-equation Turbulence Model for Aerodynamic Flows." AIAA-92-0439, 1992.

[13] Y.-Q. Shen and G.-C. Zha, "Large Eddy Simulation Using a New Set of Sixth Order Schemes for Compressible Viscous Terms ," *Journal of Computational Physics*, vol. 229, pp. 8296–8312, 2010.

[14] G.-C. Zha, Y. Shen, and B. Wang, "An improved low diffusion E-CUSP upwind scheme ," *Journal of Computer & Fluids*, vol. 48, pp. 214–220, 2011.

[15] Y.-Q. Shen and G.-Z. Zha , "Generalized finite compact difference scheme for shock/complex flowfield interaction," *Journal of Computational Physics*, vol. doi:10.1016/j.jcp.2011.01.039, 2011.

[16] Shen, Y.-Q. and Zha, G.-C. and Wang, B.-Y., " Improvement of Stability and Accuracy of Implicit WENO Scheme," *AIAA Journal*, vol. 47, No. 2, pp. 331–344, 2009.

[17] Shen, Y.-Q. and Zha, G.-C. and Chen, X.-Y., " High Order Conservative Differencing for Viscous Terms and the Application to Vortex-Induced Vibration Flows," *Journal of Computational Physics*, vol. 228(2), pp. 8283–8300, 2009.

[18] Shen, Y.-Q. and Zha, G.-C. , " Improvement of the WENO Scheme Smoothness Estimator," *International Journal for Numerical Methods in Fluids*, vol. DOI:10.1002/fld.2186, 2009.

[19] G.-C. Zha and E. Bilgen, "Numerical Study of Three-Dimensional Transonic Flows Using Unfactored Upwind-Relaxation Sweeping Algorithm," *Journal of Computational Physics*, vol. 125, pp. 425–433, 1996.

[20] B.-Y. Wang and G.-C. Zha, "A General Sub-Domain Boundary Mapping Procedure For Structured Grid CFD Parallel Computation," *AIAA Journal of Aerospace Computing, Information, and Communication*, vol. 5, No.11, pp. 2084–2091, 2008.

[21] Wang, B. Y and Zha, G.-C. , "Detached-Eddy Simulation of a Co-Flow Jet Airfoil at High Angle of Attack." AIAA Journal of Aircraft, Vol. 48, No. 5, 2011.

[22] Im, H. , Zha, G.-C., and Dano, B. P. E., "Large Eddy Simulation of Coflow Jet Airfoil at High Angle of Attack." Journal of Fluids Engineering, Vol. 136 / 021101-1, Feb. 2014.

[23] Y.-Q. Shen, G.-C. Zha, and B.-Y. Wang, "Improvement of Stability and Accuracy of Implicit WENO Scheme ," *AIAA Journal*, vol. 47, pp. 331–344, 2009.

[24] B. Dano, A. Lefebvre and G-C. Zha, "Flow mixing mechanism of a discrete co-flow jet airfoil," *AIAA paper 3097-113*, 2011.

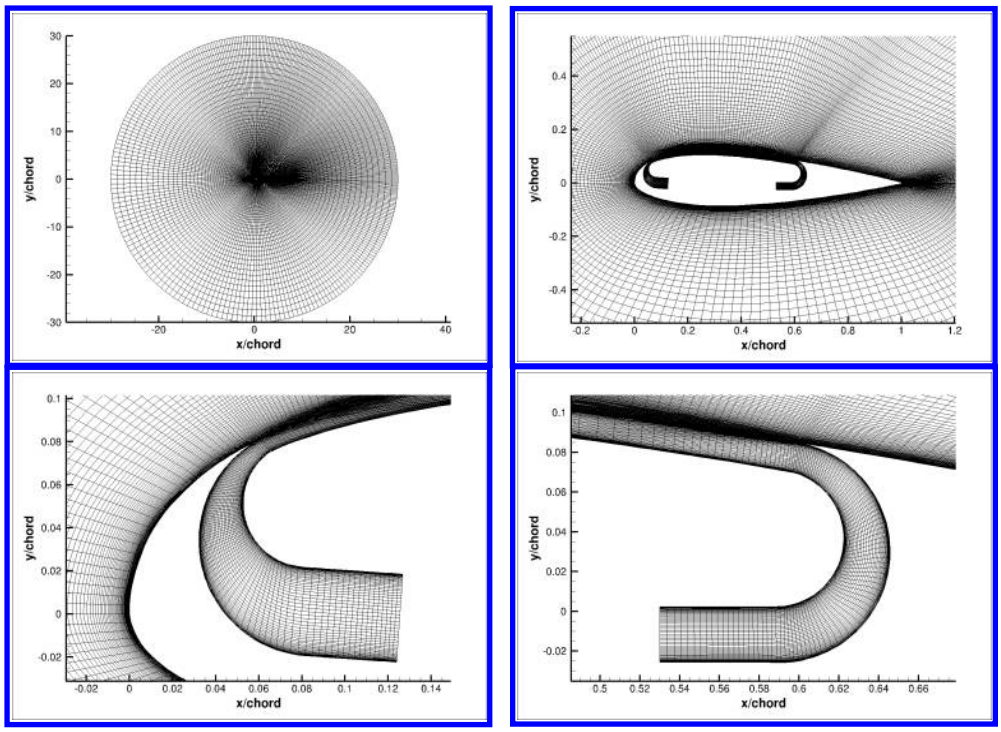

Figure 2: NACA 23121 CFJ airfoil O-mesh topology.

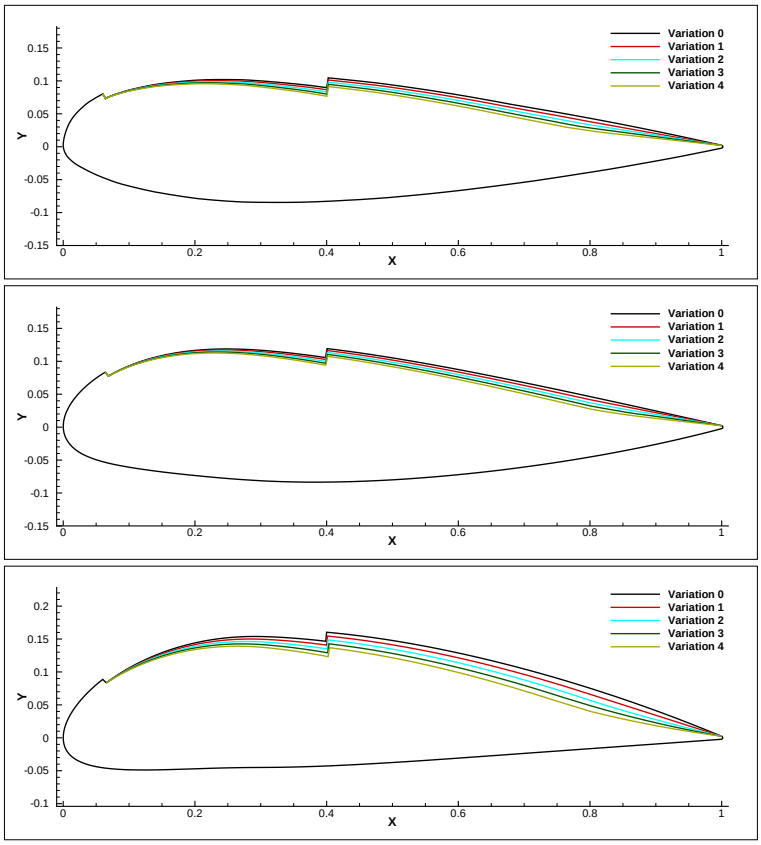

Figure 3: Geometry of the NACA 23121, NACA 34121 and NACA 6321 CFJ airfoils and their variations.

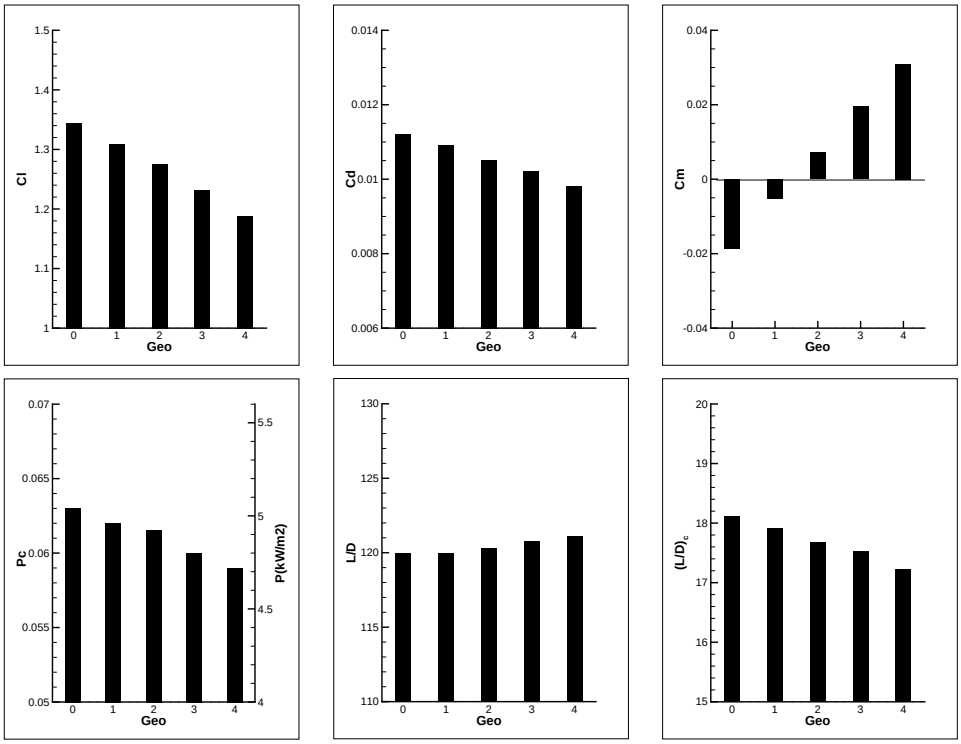

Figure 4: Variation of forces, moment and power consumption for the NACA 23121 CFJ airfoils variations at $AoA = 10^{\circ}$ and $C_{\mu} = 0.16$.

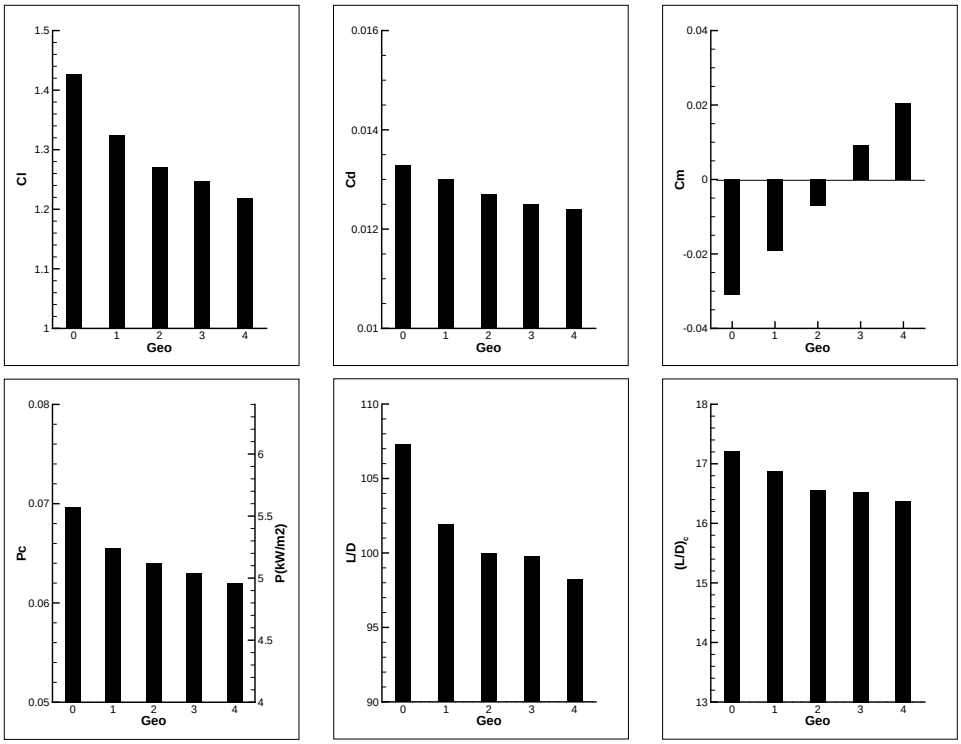

Figure 5: Variation of forces, moment and power consumption for the NACA 34121 CFJ airfoils variations at $AoA = 10^{\circ}$ and $C_{\mu} = 0.16$.

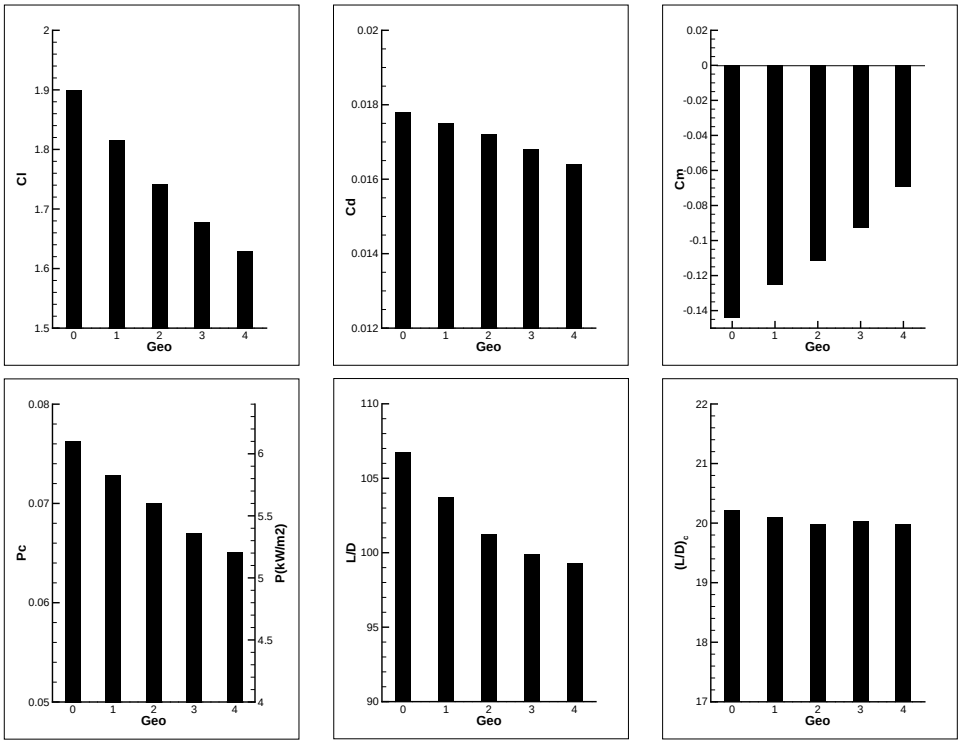

Figure 6: Variation of forces, moment and power consumption for the NACA 6321 CFJ airfoils variations at $AoA = 10^{\circ}$ and $C_{\mu} = 0.16$.

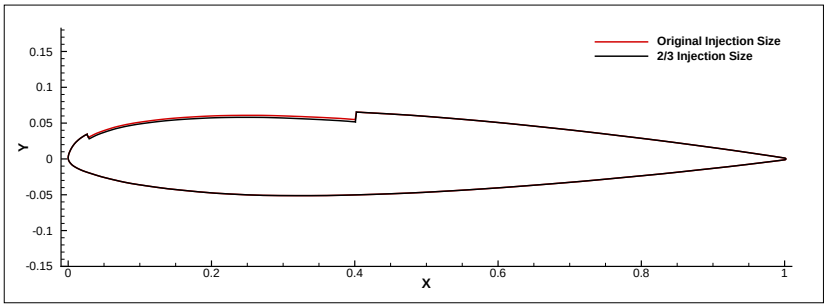

Figure 7: Geometry of the NACA 23112 CFJ airfoil with original jet size and the 2/3 jet size.

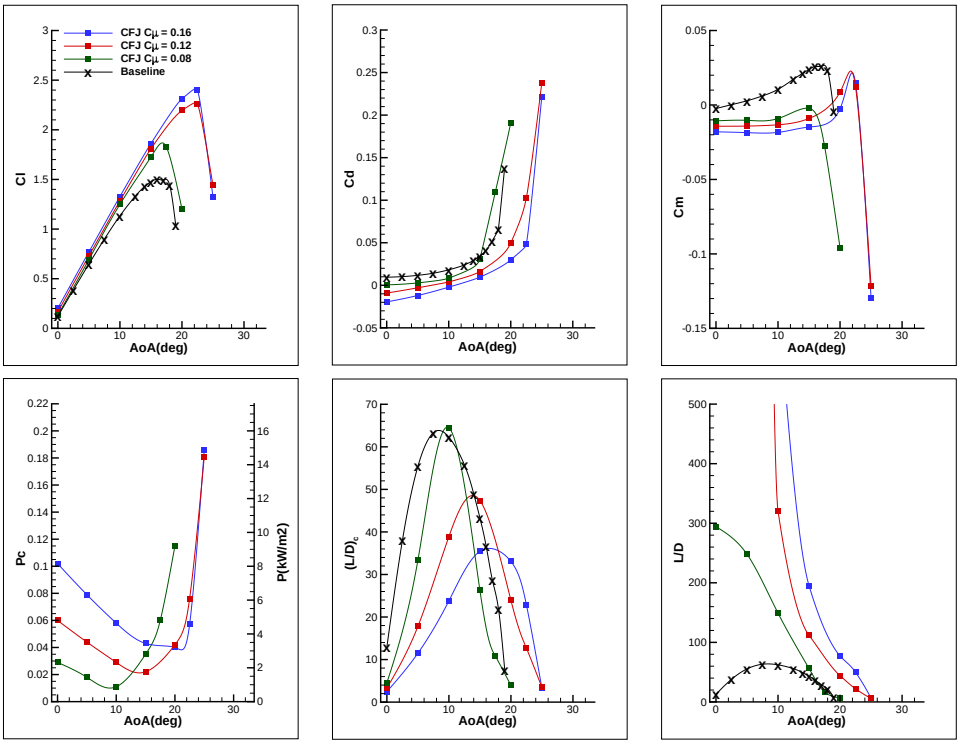

Figure 8: Variation of forces, moment and power consumption for the NACA 23112 CFJ airfoils with AoA and C_μ.

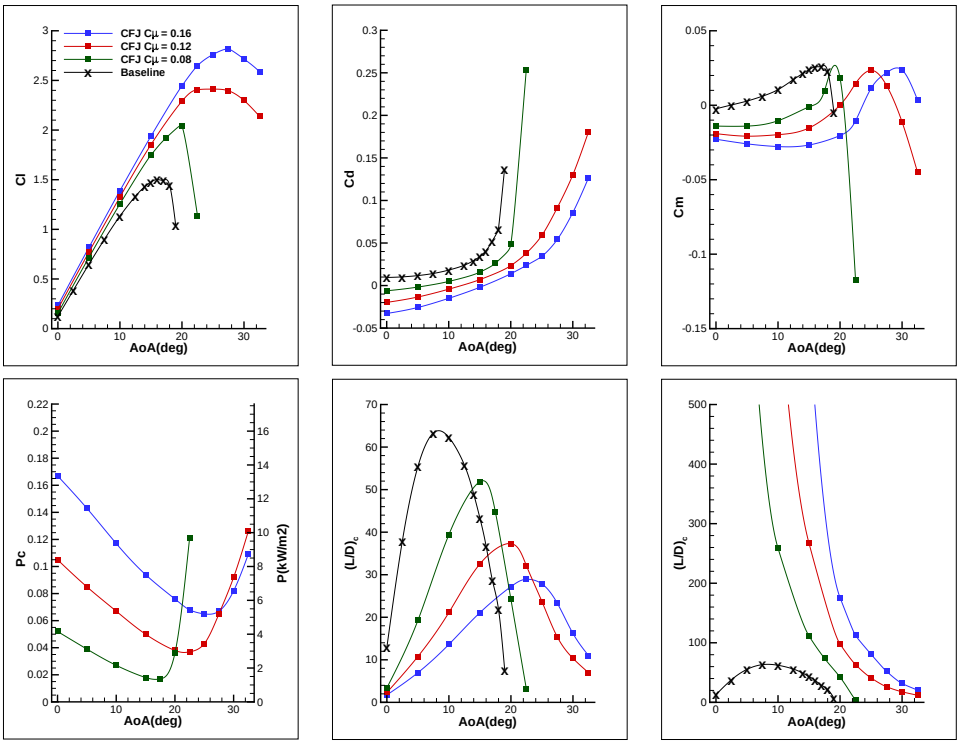

Figure 9: Variation of forces, moment and power consumption for the NACA 23112 CFJ airfoils with AoA and C_μ. The jet size is reduced to 2/3 of the original jet size.

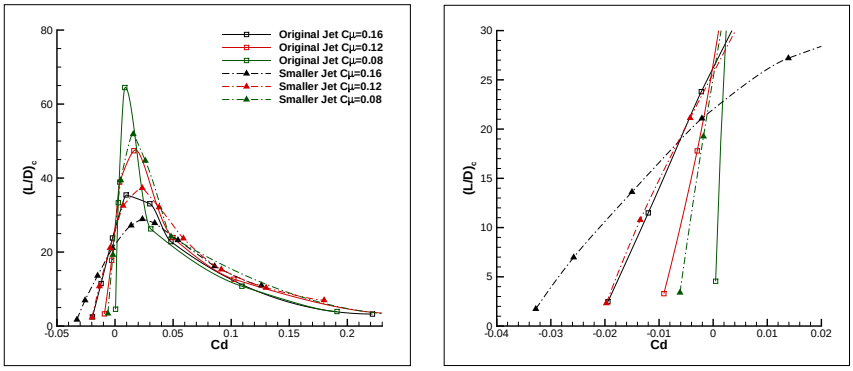

Figure 10: $(\frac{L}{D})_c$ versus C_D for the NACA 23112 CFJ airfoil with original and reduced injection sizes plotted for various C_μ. The thrust generation area is zoomed-in on the right plot.